The senescence-associated secretory phenotype mediates oncogene-induced senescence in pediatric pilocytic astrocytoma

Juliane L. Buhl[1,2,3], Florian Selt[1,3,4], Thomas Hielscher[5], Romain Guiho[6], Jonas Ecker[1,3,4], Felix Sahm[7,8], Johannes Ridinger[1,2,3], Dennis Riehl[9], Diren Usta[1,3], Britta Ismer[1,2,10], Alexander C. Sommerkamp[1,2,10], J.P. Martinez-Barbera[6], Annika K. Wefers[7,8], Marc Remke[11,12,13], Daniel Picard[11,12,13], Stefan Pusch[7,8], Jan Gronych[14], Ina Oehme[1,3], Cornelis M. van Tilburg[1,3,4], Marcel Kool[1,15], Daniela Kuhn[1,3], David Capper[7,8,16], Andreas von Deimling[7,8], Martin U. Schuhmann[17], Christel Herold-Mende[18], Andrey Korshunov[7,8], Tilman Brummer[19], Stefan M. Pfister[1,4,15], David T.W. Jones[1,10], Olaf Witt[1,3,4] and Till Milde [1,3,4*]

[1] Hopp Children's Cancer Center at the NCT Heidelberg (KiTZ), Heidelberg, Germany
[2] Faculty of Biosciences, Heidelberg University, Heidelberg, Germany
[3] Clinical Cooperation Unit Pediatric Oncology, German Cancer Research Center (DKFZ) and German Consortium for Translational Cancer Research (DKTK), Heidelberg, Germany
[4] KiTZ Clinical Trial Unit (ZIPO), Department of Pediatric Hematology and Oncology, Heidelberg University Hospital, Heidelberg, Germany
[5] Division of Biostatistics, German Cancer Research Center (DKFZ) and German Consortium for Translational Cancer Research (DKTK), Heidelberg, Germany
[6] Developmental Biology and Cancer Programme, Birth Defects Research Centre, Great Ormond Street Institute of Child Health, University College London, London, UK
[7] Department of Neuropathology, Heidelberg University Hospital, Heidelberg, Germany
[8] Clinical Cooperation Unit Neuropathology, German Cancer Research Center (DKFZ) and German Consortium for Translational Cancer Research (DKTK), Heidelberg, Germany
[9] Immune Monitoring Unit, DKFZ/NCT, Heidelberg, Germany
[10] Pediatric Glioma Research Group, German Cancer Research Center (DKFZ) and German Consortium for Translational Cancer Research (DKTK), Heidelberg, Germany
[11] Department of Pediatric Neuro-Oncogenomics, German Cancer Research Center (DKFZ) and German Consortium for Translational Cancer Research (DKTK), partner site Essen/Düsseldorf, Düsseldorf, Germany
[12] Department of Pediatric Oncology, Hematology, and Clinical Immunology and Medical Faculty, University Hospital Düsseldorf, Düsseldorf, Germany
[13] Department of Neuropathology, Medical Faculty, Heinrich-Heine University Düsseldorf, Düsseldorf, Germany
[14] Division of Molecular Genetics, German Cancer Research Center (DKFZ), Heidelberg, Germany
[15] Division of Pediatric Neurooncology, German Cancer Research Center (DKFZ) and German Consortium for Translational Cancer Research (DKTK), Heidelberg, Germany
[16] Charité - Universitätsmedizin Berlin, corporate member of Freie Universität Berlin, Humboldt-Universität zu Berlin, and Berlin Institute of Health, Department of Neuropathology, Berlin, Germany
[17] Division of Pediatric Neurosurgery, Department of Neurosurgery, University Hospital Tübingen, Tübingen, Germany
[18] Department of Neurosurgery, Heidelberg University Hospital, Heidelberg, Germany

[19] Institute of Molecular Medicine and Cell Research (IMMZ), Faculty of Medicine, University of Freiburg, Freiburg, Germany, Centre for Biological Signalling Studies BIOSS, University of Freiburg and German Consortium for Translational Cancer Research (DKTK), Freiburg, and German Cancer Research Center (DKFZ), Heidelberg, Germany

Running title: The SASP mediates OIS in pediatric PA

Key words: low-grade glioma, pilocytic astrocytoma, oncogene-induced senescence (OIS), senescence-associated secretory phenotype (SASP), IL1B

Additional information:

Financial support, including the source and number of grants, for each author:
JE received a postdoc stipend from the Medical Faculty, Heidelberg University, through the Physician Scientist Program. DR was funded by BMBF (NCT 3.0 program immunomonitoring), JPMB was supported by the Brain Tumour Charity (SIGNAL and EVEREST), Great Ormond Street Hospital Children's Charity and National Institute of Health Research Biomedical Research Centre at Great Ormond Street Hospital for Children NHS Foundation Trust and University College London. JPMB is a Great Ormond Street Hospital for Children's Charity Principal Investigator. IO was supported by funding from the German Research Foundation (DFG) to IO (Oe542/2-1) and from the H.W.&J. Hector foundation (Grant reference number: M71). TB is supported by the Deutsche Forschungsgemeinschaft through a Heisenberg professorship. DC, SMP, DTWJ and OW received financial support from The Brain Tumor Charity (The Everest Centre for Low-grade Paediatric Brain Tumours). SMP, DTWJ, and OW received financial support from the Pediatric Low-Grade Glioma Association. OW received financial support from Children's Tumor Foundation Synodos low-grade glioma initiative. OW and TM received donations from private donors (Verein für Krebskranke Kinder Odenwald; anonymous family; EMBL employees)

*Corresponding author:
Till Milde, Clinical Cooperation Unit Pediatric Oncology, German Cancer Research Center (DKFZ), Im Neuenheimer Feld 280, 69120 Heidelberg, Germany, phone: +49 6221 423387, fax: +49 6221 3579, e-mail: t.milde@kitz-heidelberg.de.

Conflict of interest disclosure statement:
The authors declare no potential conflicts of interest.

Word count: (6 055)

Total number of figures: 7, suppl. figures: 4

Total number of suppl. tables: 6

STATEMENT OF TRANSLATIONAL RELEVANCE

Prediction of the clinical course remains a challenge in pediatric pilocytic astrocytomas (PAs), and long-term tumor control can be difficult to achieve. We here for the first time provide evidence that the senescence-associated secretory phenotype (SASP) mediates oncogene-induced senescence (OIS) in pediatric PA, which is thought to drive unpredictable growth behavior. We here show that a high SASP sum score is associated with favorable progression-free survival (PFS) independent of tumor resection status. We identify two distinct patient cohorts, one with high or intermediate SASP and complete resection (100% 3-year PFS), and one with low SASP and incomplete resection (0% 3-year PFS). This is of high clinical interest, as the SASP sum score could have the potential to inform clinical decision making, a priori identifying a) patients with complete resection that never progress and b) patients with incomplete resection that always progress. Finally, harnessing the SASP therapeutically could improve tumor control.

ABSTRACT

Purpose: Pilocytic astrocytoma (PA) is the most common childhood brain tumor, characterized by constitutive MAPK activation. MAPK signaling induces oncogene-induced senescence (OIS), which may cause unpredictable growth behavior of PAs. The senescence-associated secretory phenotype (SASP) has been shown to regulate OIS, but its role in PA remains unknown.

Experimental Design: The patient-derived PA cell culture model, DKFZ-BT66, was used to demonstrate presence of the SASP and analyze its impact on OIS in PA. The model allows for doxycycline-inducible switching between proliferation and OIS. Both states were studied using gene-expression profiling (GEP), Western blot, ELISA, and cell viability testing. Primary PA tumors were analyzed by GEP and multiplex assay.

Results: SASP factors were up-regulated in primary human and murine PA and during OIS in DKFZ-BT66 cells. Conditioned medium induced growth arrest of proliferating PA cells. The SASP factors IL1B and IL6 were up-regulated in primary PA, and both pathways were regulated during OIS in DKFZ-BT66. Stimulation with rIL1B but not rIL6 reduced growth of DKFZ-BT66 cells and induced the SASP. Anti-inflammatory treatment with dexamethasone induced regrowth of senescent cells and inhibited the SASP. Senescent DKFZ-BT66 cells responded to senolytic pan-BCL inhibitors. High IL1B and SASP expression in PA tumors was associated with favorable progression-free survival.

Conclusions: We provide evidence for the SASP regulating OIS in pediatric PA, with IL1B as a relevant mediator. SASP expression could enable prediction of progression in PA patients. Further investigation of the SASP driving the unpredictable growth of PAs, and its possible therapeutic application, is warranted.

INTRODUCTION

Pilocytic astrocytoma (PA), WHO grade I, is the most frequent pediatric brain tumor (1). Activation of mitogen-activated protein kinase (MAPK) signaling by genetic aberration is detectable in nearly all cases (2, 3). Activating KIAA1549:BRAF-fusions are the most common alterations of the MAPK pathway in PAs (60-80%) (4, 5). PA tumors are characterized by slow growth without invasive properties or tendency to progress to high-grade malignancies (6, 7). However, the growth dynamics of PAs remain clinically unpredictable. In case of complete resection the 10-year event-free survival is 85%, while it is 52% or 18% in patients with subtotal or partial resection, respectively (8). Most events occur within the first few months after surgery, but regrowth of seemingly stable tumors can be observed for up to 12 years later (8).

This unpredictable clinical course possibly results from variable activity of oncogene-induced senescence (OIS), a tumor-suppressive mechanism induced by aberrant MAPK activation (9, 10). OIS prevents proliferation of malignant cells by triggering cell cycle arrest (11). The resulting growth arrest is thought to be the reason why long-term primary cultures of PAs are notoriously difficult to handle, consequently hampering the establishment of representative PA models. Establishment of patient-derived xenograft (PDX) models has been unsuccessful as a consequence of both OIS and replicative senescence. Expression of truncated BRAFV600E by RCAS-mediated gene delivery in mice induced PA-like tumors (12), which stop growing at some point and are typically not lethal. Furthermore, BRAFV600E overexpression in human neural stem cells was shown to induce initial transformation but subsequent growth arrest (10). Another murine glioma model of PA was established by transduction of either BRAFV600E or the KIAA1549:BRAF fusion in TP53 null murine neural progenitor cells (13). We have generated the first BRAF-fusion positive PA cell line derived from patient tumor material, DKFZ-BT66, by reversibly interfering with two important pathways for OIS, CDKN2A/RB1 and TP53/CDKN1A, via doxycycline-inducible expression of the SV40 large T antigen (14). This model faithfully recapitulates the molecular biology of KIAA1549:BRAF-fusion positive pediatric PAs, and enables not only the characterization of MAPK signaling under the endogenous KIAA1549:BRAF fusion, but also the analysis of OIS and its regulating signaling pathways in PA.

Markers of OIS such as SA-β-Gal positivity and up-regulation of CDKIs (p16, p21) have been described in primary PA tumors (9). The proliferative index, measured by Ki-67 staining, is 1-2% in PAs on average (15), but might be higher during the initial growth phase. OIS is possibly one of the reasons for this low proliferation rate. We have shown that elevated OIS gene expression

profile (GEP) scores in pediatric PA correlate with favorable progression-free survival (PFS) (14), pointing toward a role of OIS in maintenance of clinically stable disease.

OIS has been shown to depend on a complex inflammatory network, the senescence-associated secretory phenotype (SASP), in fibroblast models (16, 17). In these models OIS was overcome by interfering with cytokine signaling pathways (18, 19). Secretion of SASP factors is known to induce and maintain growth arrest, thereby limiting tumor progression of benign neoplasms (18). In addition, the secreted cytokines attract immune cells, leading to clearance of growth-arrested genetically altered cells (20). However, the resulting shift in tissue microenvironment also has deleterious effects. Some secreted cytokines are proangiogenic and thereby can enhance growth of neighboring cells (21, 22). Thus, the SASP can have both cancer suppressive as well as cancer promoting effects depending on the biological context. Elevated expression of miRNAs targeting genes involved in NF-kB and inflammatory signaling (23) indicate presence of the SASP in pediatric PA, but the precise role of the SASP and its mediating factors in pediatric PA is hitherto unknown.

The identification of factors regulating OIS in PA could help understand the mechanisms controlling the unpredictable growth behavior of PA tumors. This knowledge could enable both prediction of the clinical course as well as possible therapeutic interference with specific factors or pathways. Here we provide evidence of mediation of OIS by the SASP and one of its factors, IL1B, in pediatric PA and postulate that the SASP is a clinically relevant factor for stable disease in PA.

MATERIALS AND METHODS

Cell culture

DKFZ-BT66 cells (passages 8-17), containing the doxycycline-inducible SV40 large T antigen, were cultured and viability and cell counts were measured as described in (14). The identity of the cell line was confirmed by Multiplex Cell Line Authentication (MCA) test and it was proven to be free of mycoplasma or viral contamination by Multiplex cell Contamination Test (McCT) assay (http://www.multiplexion.de) (24). After generation of the cell line in our lab, the cells were tested for contamination (10/2015), aliquoted and frozen. From these stocks cells in culture were tested with Venor®GeM Classic (cat. no. 11-1250, Minerva biolabs, Berlin, Germany) for mycoplasma once a month. Normal Human Astrocytes (NHA) primary cells (passage 2) (obtained 06/2017, cat. no. CC-2565, LONZA, Basel, Switzerland) were cultured in AGM Astrocyte Growth Medium BulletKit (cat. no. CC-3186, LONZA) and tested for mycoplasma contamination monthly with the MycoAlert Mycoplasma Detection Assay (cat. no. LT07-318, LONZA).

Drugs and cytokines

Water soluble dexamethasone (cat. no. D2915, Sigma-Aldrich, St. Louis, MO, USA) was dissolved in sterile water and stored at -20°C. Anakinra (Kineret 150 mg/ml, Sobi, Stockholm, Sweden) and tocilizumab (RoActemra 20 mg/ml, Hoffmann-LaRoche, Basel, Switzerland), both dissolved in sterile water, were stored at 4°C. Recombinant IL1B and IL6 (cat. nos. 201-LB-005 and 206-IL-010, R&D Systems, Minneapolis, MN, USA) were dissolved in sterile PBS containing 0.1% BSA and stored at -80°C. Navitoclax (ABT-263, cat. no. 11500, Cayman chemical, Ann Arbor, MI, USA), ABT-737 (cat no. ab141336, Abcam, Cambridge, UK), dasatinib (cat. no. S1021, Selleckchem, Houston, TX, USA), quercetin (cat. no. S2391, Selleckchem), vincristine sulfate (cat. no. S1241, Selleckchem) and trametinib (GSK1120212, cat. no. A3018, ApexBio, Houston, TX, USA) were dissolved in DMSO. Carboplatin (cat. no. S1215, Selleckchem) was dissolved in sterile water. All drugs were dissolved as described and stored in aliquots at -80°C. Drugs and cytokines were diluted in cell culture medium and added to the cells for the durations and concentrations indicated.

Gene expression profiles (GEPs)

Generation of GEPs was performed as described previously (3). Briefly, GEP of patient samples as well as the DKFZ-BT66 cell line was done on Affymetrix U133 Plus 2.0 expression arrays, while GEP of the murine PA model was done on Affymetrix Mouse Genome 430 2.0 arrays. Expression values from patient data was MAS5 normalized. Expression values of the cell line as

well as the murine PA model were RMA normalized and log2-transformed. In case of multiple probe-sets per gene, the probe-set with highest overall expression was selected. All GEP datasets will be made publically available upon publication of the manuscript. GEP datasets used to identify OIS-controlling candidate genes were E-NCMF-12 (human fibroblasts/BRAFV600E, n=20) (18), E-NCMF-13 (human fibroblasts/BRAFV600E, n=16) (18), GSE54402 (human fibroblasts/HRASG12V, n=10) (25), GSE46801 (primary human melanocytes/BRAFV600E, n=9) (26), GSE41318 (human fibroblasts/RAS, n=6) (Acosta et al., unpublished), and GSE60652 (human fibroblasts/RAS, n=4) (27).

In vivo mouse model

Murine PA tumors were induced using the RCAS/Tv-a system as described before (12). Briefly, DF-1 cells expressing RCAS BRAFV600E were injected into the cerebral hemisphere of neonatal Nestin Tv-a (Ntv-a) mice. Age-matched non-injected Ntv-a mice were used as controls. Mice were sacrificed 5-6 weeks after injection and tumor tissue was isolated. All animal procedures were performed according to protocols approved by the German authorities (Regierungspräsidium Karlsruhe; G-69/13, DKFZ342).

Senescence-associated ß-galactosidase (SA-ß-Gal) staining

SA-ß-Gal staining was performed as described previously (14).

Conditioned medium (CM)

For conditioning of media, DKFZ-BT66 cells were seeded with or without doxycycline. Cell numbers for seeding were adjusted to end up with similar numbers (n= $2x10^6$) after five days of culturing accounting for proliferating versus senescent cells. The cell number was chosen according to ELISA results for an estimated secretion of at least 100 pg/ml of IL1B at day five. Medium was changed on day three and collected on day five, resulting in two days of conditioning. Collected medium was centrifuged and filtered (0.22µm). Freshly collected CM was supplemented with doxycycline and added every second day to DKFZ-BT66 cells.

Microscopy

Bright field pictures were taken as described before (28).

RNA isolation, cDNA synthesis and quantitative reverse transcription real-time PCR (RT-qPCR)

RNA extraction, cDNA synthesis and RT-qPCR were conducted as described previously (14). QuantiTect primers used are given in supplementary table 1.

Enzyme linked immuno-sorbent assay (ELISA)

Cytokine concentrations were measured via ELISA Kits for IL1B (cat. no. DLB50, R&D Systems) and IL6 (cat. no. D6050, R&D Systems). ELISA experiments were performed according to manufacturer's instructions. Supernatant was centrifuged before use and stored at -80°C. Cytokine concentrations (pg/ml) were normalized to cell counts in each well (cell number/ml) resulting in cytokine concentration/cell (pg/cell).

Western blot

Western blots were performed as described previously (28). Antibodies and corresponding membranes are given in supplementary table 1. Depicted blots are always representative of a least three replicates.

Cytokine measurement in primary tumors by multiplex assay ("Luminex")

Fresh frozen tumors and one normal fetal brain sample (1-3 mm^3) were lysed by Bio-Plex® Cell Lysis Kit (Bio-Rad, Hercules, CA, USA) according to the manufacturer's protocol. Total protein concentrations were determined by Pierce™ BCA Protein Assay Kit (Thermo Fisher Scientific, Waltham, MA, USA) and normalized to 1 mg/ml. n=27 different cytokines/chemokines (consisting of n=14 SASP factors and n=13 non-SASP factors) were analyzed in one sample according by Bio-Plex Pro™ Human Cytokine 27-plex Assay (Bio-Rad) to the manufacturer's protocol. Clinical parameters are summarized in supplementary table 2.

Metabolic activity

Measurement of metabolic activity was performed in 96-well flat bottom black opaque wall plates (Corning) after 72 hours of treatment using CellTiter-Glo One Solution assay (cat. no. G8461, Promega, Madison, WI, USA) following manufacturer´s instructions. DKFZ-BT66 cells were seeded five days before treatment with 500 cells/well plus doxycycline 1µg/ml (cat. no. sc-337691, Santa Cruz, Dallas, TX, USA) and 8000 cells/well without doxycycline. NHA cells were seeded 24 hours before treatment with 4000 cells/well. Luminescence was detected by FLUOstar OPTIMA automated plate reader (BMG Labtech).

Statistics and bioinformatics

For the generation of the OIS-controlling candidate gene list, six publicly available gene expression data sets (GEO: GSE54402, GSE46801, GSE60652, GSE41318, ArrayExpress: E-NCMF12, E-NCMF13) were used. For each data set separately, up-regulated genes in the OIS condition were ranked according to their moderated t-statistic based on the empirical Bayes approach (29) as implemented in the Bioconductor package limma (30). In case a gene was represented by multiple probes, the probe with the strongest effect was selected. Consistently up-regulated genes across data sets (n=332) were identified with the rank-product approach (31), which is the geometrical mean of ranks. This analysis was based on the overlap of genes measured in each data set. Significance of rank-product was tested according to (32). P-values were adjusted to control the false discovery rate using Benjamini-Hochberg correction.

The limma approach (30) was used to test for differential gene expression. Gene set enrichment analysis (GSEA) for SASP genes (17) was performed using the camera test (33). For GSEA the most specific probe set per gene was selected using the jetset algorithm (34). All analyses were performed with statistical software R 3.4.

Ingenuity pathway analysis was conducted for the 332 genes according to the user manual. A list of the correlating genes for each pathway was generated (n=36 genes in total).

The expression level of the 332 genes selected from public GEPs, the IPA pathway genes and the SASP genes were analyzed in pediatric and adult PA patient samples (n=182) (suppl. table 4, GEO: GSE16011 (35), GSE5675 (36)) and compared to the corresponding expression level in unmatched normal fetal cerebellum samples (n=5) from non-patients (GEO: GSE44971 (37)) using the R2 web-based genomics analysis and visualization platform (http://r2.amc.nl). The dataset will be made publicly available in R2 upon acceptance. Finally, only genes were considered, which could be targeted by a small molecule inhibitor or antibody and overlapped in all three candidate gene lists.

In vitro experiments were performed in a minimum of three biological replicates. All data is presented as mean ± SD. Testing for statistical significance of differences between two groups was done by unpaired Student´s t-Test with Welch´s correction, with p-values below 0.05 considered as significant. Graphs were generated using GraphPad Prism version 5.01 and Microsoft Powerpoint 2010 for Windows.

PFS was defined as time from diagnosis to recurrence or death, whichever occurred first. Distribution of PFS was estimated with the method of Kaplan and Meier and compared between groups with the log-rank test. Univariate and multivariate Cox Regression models were used to

estimate the hazard ratio and corresponding 95% confidence interval of prognostic factors. IL1B log2-expression and SASP sum score were standardized to give the hazard ratio per one standard deviation increase. Groups were based on median cut-off (IL1B) or tertiles (SASP).

RESULTS

SASP factors are up-regulated in primary PA, during OIS in PA cells and induce growth arrest

We analyzed mRNA expression of the SASP factors in human PA patient samples (n=182) and compared it to normal brain (n=5) by means of gene expression microarrays. The SASP gene set, as defined by Coppé (17), was significantly up-regulated in human PAs (Fig. 1A). Likewise, the SASP gene set was significantly up-regulated in a murine *in vivo* PA model expressing a BRAFV600E mutation (12) (n=8) compared to healthy mice of the same age (n=8) (Fig. 1B). Using the same approach we analyzed the regulation of the SASP gene set in OIS versus proliferation in our PA cell line, DKFZ-BT66. The OIS state in DKFZ-BT66 was defined at five days after doxycycline withdrawal, coinciding with enlarged cell morphology, SV40 large T antigen protein degradation, cell cycle arrest, and up-regulation of markers of senescence such as p21 as described previously (14). Comparison of the SASP gene set in OIS versus proliferation showed a significant up-regulation of the SASP gene set overall (Fig. 1C), with 38/62 (61%) of the SASP factors significantly up-regulated (Fig. 1D, suppl. table 3). To determine the secretory nature and the functional relevance of the SASP for the induction of OIS in PA, conditioned medium (CM) experiments were conducted. CM of either senescent or proliferating DKFZ-BT66 cells was administered to proliferating DKFZ-BT66 cells together with doxycycline for continuous induction of SV40 large T antigen expression. While cells treated with CM from proliferating PA cells continued to grow, treatment with CM from senescent cells induced growth arrest (Fig. 1E) as well as an enlarged cell morphology characteristic for senescence (11) (Fig. 1F). Taken together these data suggest that the SASP is up-regulated in human and murine PA as well as in our PA cell line, is secreted during OIS in DKFZ-BT66 cells and is sufficient to induce growth arrest of proliferating cells.

Identification of the OIS-controlling candidate genes IL1B and IL6 in pediatric PA

As the composition of SASP factors differs depending on tissue and cell type (16), we next investigated which SASP factors as well as other OIS-controlling genes are expressed in pediatric human PAs. In order to identify specific OIS-controlling genes for pediatric PA, we collected and generated three candidate gene lists of relevant OIS and SASP genes (Step 1), investigated the expression of these genes in primary human PA samples (Step 2) and generated a final candidate gene list after accounting for consensus in the three candidate gene

lists as well as druggability (Step 3) (Fig. 2A).

The first candidate gene list (“SASP genes”) consists of the SASP genes published by Coppé (n=62 genes) (17), accounting for the published SASP genes. The second candidate gene list (“Published OIS genes”) was generated by screening publicly available GEP datasets from six human OIS models (including RAS or BRAFV600E transduced fibroblasts and primary melanocytes) for genes up-regulated in all 6 datasets (n=332 genes). This list accounts for genes up-regulated in independent general OIS models. The third gene list ("Top IPA pathway genes”) was generated by identifying the top signaling pathways up-regulated in the “Published OIS genes” set performing ingenuity pathway analysis (IPA) and including all genes related to the respective pathways (n=36 genes). This list additionally adds all genes related to the pathways up-regulated in OIS, which may not have been included on a single gene basis. In step 2 the expression of all three candidate gene lists (“SASP genes”, “Published OIS genes”, “Top IPA pathway genes”) was analyzed in n=182 PA samples (suppl. table 4) and compared to n=5 normal brain samples, in order to identify the candidate genes relevant to PA. In a third step, we filtered for consensus candidate genes (n=5), by omitting all genes that did not appear in all three candidate gene lists. Finally, for experimental as well as therapeutical purposes, only genes which could be targeted by a small molecule inhibitor or antibody were considered, resulting in a PA-specific OIS-controlling candidate gene list of n=3 genes (IL1B, IL6, TNFRSF1B) (Fig. 2A and B). The candidates were validated in the murine *in vivo* PA model (12) and found to be up-regulated compared to healthy control animals (Fig. 2C). The PA tumors induced by BRAFV600E expression in neural progenitor cells showed up-regulated expression of CDKN2A on mRNA level compared to healthy controls (suppl. Fig. 1A), and cells derived from the PA tumors were positive for SA-ß-Gal staining (suppl. Fig. 1B). These data indicate that the murine PA model indeed displays markers of senescence and SASP expression.

While the increased mRNA expression was validated by gene expression profiling in DKFZ-BT66 in OIS for all three OIS-controlling candidate genes (Fig. 2D), RT-qPCR during OIS induction could confirm the mRNA increase only for IL1B and IL6 but not for TNFRSF1B (Fig. 2E). IL1B and IL6 are both secreted into the supernatant, as detected by ELISA (Fig. 2F). Up-regulation of IL1A/B and IL6 has previously been described in other senescence models in fibroblasts (18, 38-40), human epithelial cells (16), BRAFV600E transduced human melanocytes (18), and prostate epithelial cancer cells (16), suggesting that IL1B and IL6 are important regulators of OIS. We therefore focused on IL1B and IL6 as OIS-controlling candidate genes in PA in the further analyses.

IL1 and IL6 signaling pathways are present and regulated during OIS in PA

As we detected up-regulation and secretion of IL1B and IL6 during induction of OIS, we next aimed at elucidation of their function during OIS in PA. In a first step, the expression and activation of the IL1B and IL6 signaling cascades were determined in DKFZ-BT66 and in primary pediatric PA tumors. The IL1R1 receptor is expressed on mRNA and protein level in DKFZ-BT66 cells (Fig. 3A and B), but no significant regulation was detected. While the activity of IL1B signaling is regulated by a variety of mechanisms, its receptor is indeed rarely up-regulated in disease models (41). To determine activation of the IL1 pathway, protein expression of the downstream targets IRAK1 and phosphorylation of p65 was investigated. IRAK1, the interleukin-1 receptor-associated kinase 1, is phosphorylated and degraded upon activation of the IL1 pathway (42). Degradation of IRAK1 was indeed observed after induction of senescence and subsequent growth arrest in DFKZ-BT66 cells (Fig. 3B). NF-kB, a transcription factor highly associated with OIS has been shown to be an important regulator of the SASP (43, 44). Activation of NF-kB was assessed by phosphorylation status of p65, which increased after OIS induction in DKFZ-BT66 cells (Fig. 3B). In conclusion, the IL1 pathway is active during OIS in the DKFZ-BT66 cell model.

The IL6Ra receptor is expressed on mRNA and protein level in DKFZ-BT66 cells (Fig. 3C and D). While no significant changes were observed on mRNA level (Fig. 3C), the protein levels decreased during OIS induction (Fig. 3D). It has been described that long-term activation of the IL6 pathway initiates a negative feedback loop, leading to internalization and degradation of IL6Ra (45). In parallel we detected reduction of IL6 signaling during OIS induction in DKFZ-BT66 cells as measured by reduced phosphorylation of the downstream target STAT3 (p-STAT3) in comparison to initial levels (Fig. 3D). Activation of the IL6 pathway leads to phosphorylation of STAT3 within minutes (46), while long-term activation induces negative feedback and leads to down-regulation of p-STAT3 (47). We conclude that the initial activity of the IL6 pathway is down-regulated in our PA cell culture model, possibly due to continuous IL6 secretion during induction of OIS and subsequent growth arrest.

Expression of IL1B and IL6 protein was analyzed in n=22 pediatric PA samples and one normal brain sample by multiplex assay and both cytokines were detected in every sample (Fig. 3E).

Taken together, these data indicate that the IL1 as well as the IL6 pathway is regulated during OIS in our PA model, but only the IL1 pathways remains activated while a negative feedback regulation of the IL6 pathway is observed. Both cytokines are present in primary pediatric PA.

IL1B but not IL6 signaling reduces proliferation of PA cells and induces SASP expression

After observing elevated IL1B and IL6 levels during OIS, we next determined the role of both cytokines for OIS induction. Increasing concentrations of recombinant cytokines rIL1B and rIL6 were used to actively stimulate both pathways in proliferating DKFZ-BT66 cells.

Treatment with rIL1B resulted in significant reduction of proliferation of DKFZ-BT66 cells in a concentration dependent manner, without affecting cell viability (Fig. 4A, suppl. Fig. 2). Increasing concentrations of rIL1B above 100 pg/ml could not maximize the resulting growth reduction. The IL1 pathway was activated by rIL1B treatment, evident by degradation of IRAK1 as well as elevated protein levels of the precursor form of IL1B (31 kDA) (Fig. 4B). Elevation of IL1B due to de novo translation after positive feedback activation has been described previously (48). Of note, the maximum reduction of both proliferation and of IRAK1 protein was seen at the same concentration of rIL1B (100 pg/ml), indicating a strong correlation between IL1 pathway activity and cell proliferation. On the contrary, no significant effect on proliferation of DKFZ-BT66 cells was detected upon treatment with rIL6 (Fig. 4C). The IL6 pathway was indeed activated after short-term treatment with rIL6, as observed by elevated phosphorylation of STAT3 in a concentration dependent manner, excluding unsuccessful stimulation of the pathway (Fig. 4D).

As the SASP is a complex mixture of inflammatory signaling molecules acting in a concerted fashion, we tested if combination treatment of rIL1B and rIL6 has an additional or synergistic effect on cell proliferation. Co-treatment resulted in a significant down-regulation of cell growth in comparison to solvent control, however depending only on the concentration of rIL1B (Fig. 4E). Addition of rIL6 in increasing concentrations did not lead to additional reduction in cell growth.

The IL1 pathway was active for the entire duration (up to day 20) of the experiment as detected by IRAK1 degradation (Fig. 4F). SV40 large T antigen was expressed throughout the experiment and its downstream signaling resulted in reduced expression of p21 (Fig. 4F). Thus, the inhibitory effect of IL1B on cell proliferation is not based on alterations in SV40 large T antigen and subsequent p21 expression. As previously described SA-β-Gal cannot be used as senescence marker in DKFZ-BT66 (14). However, enlarged cellular morphology characteristic

for senescence was observed after treatment with rIL1B (Fig. 4G). Additionally, significant up-regulation of the SASP factors was determined by GEP under treatment with rIL1B (Fig. 4H).

In summary, IL1B, but not IL6, induces growth arrest of proliferating PA cells, and IL1B induces senescent morphology and up-regulation of the SASP factors. We conclude that IL1B plays an important role in induction of SASP-mediated OIS in PA.

Interference with inflammatory signaling, but not with IL1 signaling alone, leads to suppression of the SASP and growth of senescent PA cells

Having identified IL1B as important for senescence induction, we next assessed the role of IL1B for OIS maintenance. Senescent DKFZ-BT66 cells were treated with anakinra, an antagonist of the IL1 receptor. OIS-induced growth arrest could not be circumvented by treatment with anakinra alone, as determined by cell counts over the course of 20 days (Fig. 5A). IL1B signaling was inhibited, as shown by rescued IRAK1, pro-IL1B and p-p65 levels (Fig. 5B). Pharmacological inhibition of the IL1 signaling pathway alone therefore cannot bypass OIS in our model, similar to reports in other OIS models (18).

As inhibition of single SASP factors did not suffice to overcome growth arrest of PA cells in OIS, we attempted to bypass OIS by treatment with dexamethasone, a broad anti-inflammatory drug, known to inhibit the SASP (49, 50). Treatment of senescent DKFZ-BT66 cells with 100 nM dexamethasone for 20 days resulted in a significant increase in cell proliferation compared to solvent control (Fig. 5C). Exemplary for SASP factors, dexamethasone strongly inhibited the IL1 pathway as determined by rescued protein levels of IRAK1 (Fig. 5D). Treatment of DKFZ-BT66 cells in OIS with dexamethasone for five days led to a significant reduction in expression of SASP factors as determined by GEP, illustrated in the GSEA (Fig. 5E). IPA analysis of the GEPs revealed IL1B as the top upstream regulator, predicted to be inhibited under dexamethasone treatment (suppl. table 5). Importantly, of the top five upstream regulators identified by IPA in either senescent DKFZ-BT66 cells treated with dexamethasone or in proliferating DKFZ-BT66 cells treated with rIL1B, 4/5 were identical (IL1B, TREM1, TNF, NF-kB complex) and regulated in an opposite fashion (inhibition vs. activation) (Fig. 5F). This suggests similar SASP pathways to be involved in IL1B-induced senescence and reversal of senescence by dexamethasone, in an opposite manner. In summary these data indicate that bypass of SASP-mediated OIS-induced growth arrest is possible by inhibiting multiple SASP pathways with an anti-inflammatory drug in PA cells.

IL1B and the SASP are expressed in primary PAs and predict favorable progression-free survival independent of tumor resection status

The SASP as well as IL1B play a significant role in the regulation of OIS in our PA cell model and could mediate the variable growth behavior of pediatric PAs observed clinically. In order to assess the clinical relevance of our findings we analyzed the expression of IL1B and the SASP in primary pediatric PA samples. Using a multiplex assay, all n=14 SASP factors present in the assay were detected in primary PAs on protein level (suppl. Fig. 3). To test for a correlation between SASP factor mRNA expression and clinical outcome in PA patients, the ICGC PedBrain PA cohort (n=112 patients; survival data available for 110/112 patients (98.2%) (3), for annotations see suppl. table 4) was analyzed for expression of IL1B as well as by means of a SASP sum score (SASP score), which sums up the expression levels of all SASP factors for one patient. Increased expression of IL1B alone (both as continuous or grouped variable according to median cut-off) predicted favorable prognosis (e.g. continuous variable: HR=0.4, 95%CI 0.24-0.69, p=0.0008; n=110 patients, suppl. table 6). IL1B remained a factor for good prognosis in a multivariate analysis after accounting for other significant prognostic factors such as extent of tumor resection (HR=0.37, 95%CI 0.18-0.75, p=0.0056; n=90 patients, suppl. table 6) or radiation therapy (HR=0.35, 95%CI 0.15-0.77, p=0.0079; n=75 patients, suppl. table 6). 5-year progression-free survival (PFS) was 85% in the "IL1B high" group versus 46% in the "IL1B low" group, and survival differed significantly (log-rank test) (Fig. 6A). Similarly, patients with a higher SASP score (continuous variable) had a significantly more favorable PFS (HR=0.56, 95%CI 0.34-0.93, p=0.026, n=110 patients; suppl. table 6). The prognostic effect of the SASP score remained significant in a multivariate analysis after accounting for other significant prognostic factors such as extent of resection (HR=0.36, 95%CI 0.16-0.82, p=0.01; n=90, suppl. table 6) or radiation therapy (HR=0.19, 95%CI 0.06-0.52, p=0.0006; n=75 patients, suppl. table 6), or both (HR=0.19, 95%CI 0.03-0.72, p=0.0100; n=58 patients, suppl. table 6). When patients were grouped into three groups according to SASP score tertiles, the 5-year PFS was 48% for the "SASP low" group, 61% for the "SASP intermediate" group and 90% for the "SASP high" group, and survival differed significantly (log-rank test) (Fig. 6B). Since resection status is a strong prognostic factor we analyzed PFS separately for either gross total resection (GTR) or sub-total resection (STR). The 5-year PFS was 100% for patients with GTR in the "SASP high" and “SASP intermediate” group versus 63.3% in the "SASP low" group, and survival differed significantly (log-rank test) (Fig. 6C). On the contrary, patients with STR in the "SASP low" group showed a particularly poor 2- and 3-year PFS of 52% and 0%, respectively (Fig. 6D).

In conclusion, SASP factors are expressed on mRNA and protein level in primary pediatric PAs. Elevated mRNA expression of SASP factors correlates with a high probability to remain progression-free, and low expression of SASP factors correlates with a high risk of recurrence, especially in sub-totally resected cases.

Senescent DKFZ-BT66 cells are more responsive to senolytic pan-BCL inhibitors than proliferating cells

The low proliferation index observed in PAs (15) suggests that most of the tumor cells persist in a senescent state and thus are unlikely to respond to standard chemotherapeutic agents relying on cell division for their effect. To investigate the targetability of senescence in PA, we performed a drug screen in DKFZ-BT66 cells in OIS and proliferation testing single agents and combination treatments of several senolytic agents, standard of care chemotherapeutics and a MEK inhibitor. Senescent DKFZ-BT66 cells showed increased sensitivity to navitoclax and ABT-737 (both pan-BCL inhibitors) in comparison to proliferating cells. We did not observe elevated sensitivity to the combination of dasatinib and quercetin (Fig. 7A-C), as has been previously described for other senescent cells (51). Primary human astrocytes, which served as control, responded at high concentrations only (suppl. Fig. 4A-G). No significant response to carboplatin, vincristine or trametinib was detected in senescent DKFZ-BT66 cells (Fig. 7D-F). In contrast to carboplatin, vincristine reduced metabolic activity in proliferating DKFZ-BT66 cells. As the SV40 large T antigen inhibits p53 signaling in proliferating DKFZ-BT66 cells, carboplatin cannot induce p53-dependent apoptosis. Therefore the lack of effect is expected and due to the specifics of this model, but not indicative of resistance. An increase in metabolic activity in both proliferating and senescent DKFZ-BT66 cells was observed under trametinib treatment, as we have described before (14).

Navitoclax is currently being tested in several clinical trials and was evaluated as safe and well tolerated with dose-dependent thrombocytopenia as major adverse event (52). We therefore investigated the combination of navitoclax with standard of care treatment for PA patients. In our screen, we observed additive effects in the combination treatments compared to carboplatin, vincristine or trametinib alone. No antagonistic effect was detected (Fig. 7G-I). Similar results were observed for ABT-737 in combination treatments (suppl. Fig. 4H-J). In conclusion, addition of a pan-BCL inhibitor to the standard of care treatment regimen for PA patients could help eradicate senescent PA cells, which do not respond to chemotherapy and might be the source of tumor recurrence or progression at a later time point.

DISCUSSION

We here present data showing that the SASP mediates OIS in pediatric PA, and that one of the SASP factors, IL1B, significantly contributes to OIS induction. In line with our hypothesis that SASP mediates OIS and modulation of OIS plays a role in the growth dynamics of primary PA tumors, we provide evidence that expression of IL1B alone as well as overall expression of SASP factors defines PA patient cohorts with highly differing outcome. This data supports and extends upon our previous findings showing that high expression of an OIS gene signature predicts good prognosis in PA patients (14).

In the present study, SASP factors were found to be up-regulated in primary human as well as murine PA tumors. Upon induction of OIS in the cell line DKFZ-BT66, we detected significant up-regulation of the SASP factors. The SASP genes have indeed been described to be regulated on a transcriptional level (53). Our approach revealed two cytokines, IL1B and IL6, as candidate SASP factors specific for OIS regulation in PA. Indeed, upon induction and throughout OIS the IL1 pathway was activated, while OIS induction led to increased IL6 expression, which in short-term leads to activation of the IL6 signaling pathway. However, increased IL6 expression was followed by down-regulation of IL6 signaling over time in OIS, in line with known mechanisms of negative feedback for IL6 (45). Both cytokines have already been described to play an important role in OIS (18, 38). The activation of NF-kB downstream of IL1B leads to the transcription of many SASP factors, including IL1B itself, reinforcing OIS (43, 54). We were able to recapitulate the IL1 autocrine feedback activation in our model during OIS and upon rIL1B treatment. While stimulation of the IL1 pathway alone significantly reduced growth of proliferating DKFZ-BT66 cells and induced SASP gene expression as well as the OIS-characteristic cell morphology, treatment with IL6 had no effect on cell proliferation. Conversely, inhibition of the IL1 signaling pathway using the receptor antagonist anakinra was not sufficient to circumvent growth arrest in our PA model. Indeed, it has previously been shown in fibroblast OIS models that pharmacological inhibition of single inflammatory pathways did not lead to bypass of OIS (18). Our results underline the importance of the IL1 pathway as part of the SASP for the induction of OIS in PA cells, but also indicate that IL1B acts in concert with other SASP factors, since inhibition of a single SASP factor in the presence of all other SASP factors was not sufficient to overcome OIS. Treatment with the broad anti-inflammatory drug dexamethasone, however, induced proliferation, exemplary inhibition of the IL1 pathway, and suppression of the SASP in DKFZ-BT66 cells in OIS. These results are in line with previously published data indicating that the SASP is inhibited by glucocorticoids (49, 50). As dexamethasone is a drug commonly used in pediatric clinical practice, this result is potentially of high clinical relevance. Taken together,

these results demonstrate that the SASP plays a significant role in induction and maintenance of OIS. While induction of a senescent phenotype can be mediated by single factors such as IL1B in the absence of other SASP factors, the effect of the full SASP on OIS cannot be reversed by affecting single pathways, but only by treatment with e.g. broad anti-inflammatory drugs such as dexamethasone. Follow-up studies are warranted to assess the clinical impact of the use of anti-inflammatory (and immunosuppressive) drugs such as e.g. dexamethasone in pediatric PA patients.

Analysis of mRNA expression of the SASP in primary PA revealed an improved PFS for patients with a high IL1B as well as high SASP factor expression, independent of extent of tumor resection and radiation. This was particularly striking in two patient populations: 1) none of the patients with high and intermediate SASP factor expression and GTR had a tumor progression, 2) patients with STR and low SASP expression always progressed. These results could potentially have an impact on the therapeutic management and follow-up (FU) of these patient groups: 1) patients with a high or intermediate SASP sum score and GTR could potentially have longer FU intervals or even a shorter FU period overall, 2) patients with initially subtotal resection and low or intermediate SASP sum score could benefit from a complete re-resection or possibly adjuvant therapy, to improve their PFS. The prognostic significance of the SASP sum score of course needs to be validated first in a prospective manner in upcoming clinical trials.

An intriguing aspect only partially explored in this study is the prospect of therapeutical exploitation of the SASP and OIS. Senolytic agents showed activity specifically in senescent PA cells, while having no relevant effect on normal cells. This avenue could be exploited to specifically target dormant senescent PA cells not amenable to conventional chemotherapy.

Although our data is characterized in the DKFZ-BT66 cell line, and at least partially validated in primary human and murine PA tumors, it would be highly desirable to validate the cell line data in further PA cell lines with either BRAF fusions or other MAPK alterations. The current lack of appropriate models beyond DKFZ-BT66 prevents reproduction in a second cell line, and as such represents a limitation of this study, highlighting the urgent need for new additional models at the same time.

In summary, our data demonstrate presence of the SASP in PA, and its relevance as a strong regulator of PA tumor growth. The SASP can induce growth arrest in proliferating PA cells, while suppression of the SASP by anti-inflammatory treatment leads to bypass of growth arrest. The SASP factor IL1B is an important but not the singular mediator of OIS induction. The clinical

579 relevance of the SASP is demonstrated by outcome prediction by the SASP sum score, as well
580 as IL1B expression alone, independent of resection status.

Acknowledgments

We thank the patients and families for consenting to use the tumor material for this study. We thank Anne Kittler, Carina Müller, Laura Doerner, Hai Yen Nguyen, Andrea Wittmann, Ludmila Umansky and Elvira Hallauer for excellent technical assistance. We thank the microarray unit of the DKFZ Genomics and Proteomics Core Facility for performing the gene expression array analysis.

FIGURE LEGENDS:

Figure 1. Up-regulated SASP factors in pediatric pilocytic astrocytoma cells induce growth arrest. A) Barcode plot of gene set enrichment analysis (GSEA) depicting significant up-regulation of the SASP genes in PA patient samples (n=182) versus fetal normal brain (n=5). B) Barcode plot of GSEA depicting significant up-regulation of the SASP genes in the murine PA model (n=8) versus normal brain of healthy mice of the same age (n=8). C) Barcode plot of GSEA depicting significant up-regulation of the SASP genes in DKFZ-BT66 cells in OIS versus proliferation. D) Volcano plot depicting all probe sets regulated in DKFZ-BT66 during OIS, as compared to proliferation. E) Cell count of proliferating DKFZ-BT66 cells treated with conditioned medium (CM) every second day from DKFZ-BT66 cells in proliferation (blue) or OIS (red), supplemented with doxycycline (1 µg/ml) for 20 days. Depicted are mean +/- SD of three independent experiments. Significant differences are indicated as * $p<0.05$ (Student´s t-Test). F) Light microscopic comparison of DKFZ-BT66 cells grown under CM from proliferating or senescent (OIS) DKFZ-BT66 cells (as in E) at day 20.

Figure 2. Validation of OIS-controlling candidate genes in pediatric pilocytic astrocytoma. A) Graphical workflow: in step 1, OIS-controlling candidate genes were identified from published SASP factors (n=62), from publicly available OIS datasets (n=332), and related up-regulated IPA pathway genes (n=38). In Step 2 the candidate gene lists were screened for genes up-regulated in primary PA, as compared to normal brain. In step 3, a final OIS-controlling candidate gene list was generated by filtering for consensus in all three datasets and for druggability (n=3). B) Boxplot of log2 mRNA expression of the final OIS-controlling candidate genes in primary PAs (n=182) versus normal brain (NB) (n=5), analyzed in R2. Depicted are median (black bar), quartiles (box), median +/- 1.5 IQR (interquartile range) (whiskers), and outliers (circles). C) Boxplot of log2 mRNA expression of OIS-controlling candidate genes in the murine PA model (n=8) versus normal brain (NB) of healthy control mice (n=8). Depicted are median (black bar), quartiles (box), median +/- 1.5 IQR (interquartile range) (whiskers), and outliers (circles). D) Boxplot of log2 mRNA expression of OIS-controlling candidate genes in DKFZ-BT66 cells in OIS (n=3) versus proliferation (n=3), as measured by gene expression profiling. Depicted are median (black bar), quartile (box) and median +/- IQR (whiskers). E) Fold change of IL1B and IL6 transcript levels measured by RT-qPCR during induction of OIS in DKFZ-BT66 cells in comparison to expression levels of DKFZ-BT66 cells in proliferation (=day 0). Depicted are mean +/- SD of three independent experiments. F) IL1B and IL6 protein secretion measured in

the supernatant of DKFZ-BT66 cells upon OIS induction by ELISA. Concentration was normalized to cell number on the day of collection (pg/cell). Depicted are mean +/- SD of three independent experiments. Significant differences are indicated as * p<0.05; ** p<0.01; *** p<0.001 (Student´s t-Test).

Figure 3. Functional validation of the IL1 and IL6 signaling pathways during OIS. A) Fold change of IL1R1 transcript levels were measured by RT-qPCR in DKFZ-BT66 upon OIS induction relative to levels during proliferation (=day 0). Depicted are mean +/- SD of three independent experiments. B) IL1 pathway activity was determined by protein levels of IL1R1, IRAK1, phospho-p65 and p65 in DKFZ-BT66 upon OIS induction measured by western blot. Actin serves as loading control. C) Fold change of IL6Ra transcript levels as measured by RT-qPCR in DKFZ-BT66 upon OIS induction relative to levels during proliferation (=day 0). Depicted are mean +/- SD of three independent experiments. D) IL6 pathway activity was determined by protein levels of IL6Ra and pSTAT3/STAT3 upon OIS induction measured by western blot. Actin serves as loading control. E) Presence of IL1B and IL6 protein was detected by multiplex assay in all studied fresh frozen primary PA samples (black) (n=22) and in normal fetal brain (grey) (n=1). Depicted is mean +/- SD. Dots indicate values of individual samples.

Figure 4. IL1B signaling contributes to reduced PA cell proliferation and induces expression of SASP factor. A) Cell count of proliferating DKFZ-BT66 cells under rIL1B treatment in concentrations indicated for 20 days. Depicted are mean +/- SD of three independent experiments. Significant differences are indicated as * p<0.05 (Student´s t-Test). B) Protein levels of IRAK1 and pro-IL1B were determined by western blot under stimulation with rIL1B in the depicted concentrations for 4 hours in DKFZ-BT66 cells in proliferation. Actin serves as loading control. C) Cell count of proliferating DKFZ-BT66 cells under rIL6 treatment in concentrations indicated for 20 days. Depicted are mean +/- SD of three independent experiments. D) Protein levels of pSTAT3 and STAT3 were determined by western blot under stimulation with rIL6 in the depicted concentrations for 15 minutes in DKFZ-BT66 cells in proliferation. Actin serves as loading control. E) Cell count under combination treatment with rIL1B and rIL6 in the depicted concentrations for 20 days. Depicted are mean +/- SD of three independent experiments. Significant differences are indicated as * p<0.05 (Student´s t-Test). F) Protein levels of IRAK1, p21 and SV40 measured by western blot after long-term treatment with

rIL1B (500 pg/ml) (+) for 0, 5, 10 and 20 days versus solvent control (-) treatment in DKFZ-BT66 in proliferation. Actin serves as loading control. G) Light microscopic comparison of DKFZ-BT66 cells grown under treatment with 500 pg/ml rIL1B versus solvent control at day 20. H) Barcode plot of GSEA depicting significant up-regulation of the SASP genes in DKFZ-BT66 cells under treatment with 500 pg/ml rIL1B and doxycycline for five days versus DKFZ-BT66 cells in proliferation.

Figure 5. Inhibition of inflammatory signaling during OIS, but not IL1B alone, suppresses the SASP and leads to bypass of OIS. A) Cell count of senescent DKFZ-BT66 cells under anakinra treatment in the depicted concentrations for 20 days. Cells were cultured without doxycycline 5 days prior to treatment as well as throughout the duration of the entire experiment. Shown are mean +/- SD of three independent experiments. B) Protein levels of IRAK1, pro-IL1B, p-p65 and p65 determined by western blot in DKFZ-BT66 cells in OIS treated with rIL1B (500 pg/ml) +/- anakinra (20 µg/ml) for 4 hours. Actin serves as loading control. C) Cell count of senescent DKFZ-BT66 cells treated with 100 nM dexamethasone (dexa) or solvent control (0 nM dexa) for 20 days. Cells were cultured without doxycycline 5 days prior to treatment as well as throughout the duration of the entire experiment. Depicted are mean +/- SD of three independent experiments. Significant differences are indicated as * $p<0.05$, *** $p<0.001$ (Student´s t-Test). D) Protein levels of IRAK1 determined by western blot in DKFZ-BT66 cells in OIS treated with 100 nM dexamethasone (dexa) (+) or solvent control (-) for 0, 5, 10 and 20 days. Actin serves as loading control. E) Barcode plot of GSEA reveals significant down-regulation of the SASP genes in DKFZ-BT66 cells in OIS under treatment with dexamethasone (dexa) for five days. F) IPA analysis of GEPs of DKFZ-BT66 cells in OIS treated with 100 nM dexamethasone (n=3 replicates) compared to proliferating DKFZ-BT66 cells (n=3 replicates) (red, OIS + dexa), or DKFZ-BT66 cells in proliferation treated with 500 pg/ml rIL1B (n=3 replicates) compared to DKFZ-BT66 cells in OIS (n=3 replicates) (blue, proliferation + rIL1B) for five days. The 4 common genes of the top 5 upstream regulators of each condition are displayed. The z-score predicts the activation status of the upstream regulator, positivity indicates activation, negativity indicates inhibition. Color indicates from which condition the z-score was calculated. White bar: z-score for TREM1 in the OIS + dexa condition did not pass the threshold to indicate its inhibition/activation.

Figure 6. SASP factor expression predicts PFS independent of resection status implying a crucial role of inflammatory signaling for PA tumor growth behavior. A) Kaplan-Meier analysis of PA patients (n=110) depicting superior progression-free survival (PFS) in the IL1B mRNA high expression group ("IL1B high") (p=0.006, log-rank). B) Kaplan-Meier analysis with PA patients (n=110) grouped into three groups according to SASP score tertiles, depicting significantly different PFS (p=0.02, log-rank). C) Kaplan-Meier analysis, only PA patients with gross total resection (GTR) (n=61) are shown depicting significantly different PFS (p=0.047, log-rank). Both “SASP high” and “SASP intermediate” have no events and curves are fully overlapping. D) Kaplan-Meier analysis, only patients with sub-total resection (STR) (n=32) are shown. Panel A-D all depict patients from the same PA cohort from ICGC PedBrain (PFS available for n=110/112, 98.2%). Information on resection status was available for n=93/110 (84.5%) patients of the ICGC PA cohort.

Figure 7. Senescent DKFZ-BT66 cells respond to senolytic agents. A - F) Assessment of metabolic activity by CellTiter-Glo of senescent (red) or proliferating (blue) DKFZ-BT66 cells treated for 72 hours with navitoclax (A), ABT-737 (B), dasatinib plus quercetin (C), carboplatin (D), vincristine (E) and trametinib (F) in the indicated concentrations. Shown are mean +/- SD of three technical replicates. IC50 concentrations are depicted for DKFZ-BT66 cells in OIS (red) and in proliferation (blue). NA = not available. G – I) Assessment of metabolic activity by CellTiter-Glo of senescent (red) or proliferating (blue) DKFZ-BT66 cells treated for 72 hours with navitoclax in combination with carboplatin (G), vincristine (H), or trametinib (I) in the indicated concentrations. Shown are mean +/- SD of three technical replicates.

Supplementary table legends

Suppl. table 1. Primers & Antibodies

Suppl. table 2. Clinical annotations of the multiplex assay PA cohort and normal brain

Suppl. table 3. GEP results of SASP in DKFZ-BT66 in OIS vs. proliferation

Suppl. table 4. Clinical annotation of the PA patient cohort

Suppl. table 5. IPA upstream regulators

Suppl. table 6. Uni- and multivariate analysis of IL1B and SASP in the PA cohort

References

1. Ostrom QT, Gittleman H, Liao P, Vecchione-Koval T, Wolinsky Y, Kruchko C, et al. CBTRUS Statistical Report: Primary brain and other central nervous system tumors diagnosed in the United States in 2010-2014. Neuro-oncology. 2017;19:v1-v88.
2. Zhang J, Wu G, Miller CP, Tatevossian RG, Dalton JD, Tang B, et al. Whole-genome sequencing identifies genetic alterations in pediatric low-grade gliomas. Nature genetics. 2013;45:602-12.
3. Jones DT, Hutter B, Jager N, Korshunov A, Kool M, Warnatz HJ, et al. Recurrent somatic alterations of FGFR1 and NTRK2 in pilocytic astrocytoma. Nature genetics. 2013;45:927-32.
4. Jones DT, Kocialkowski S, Liu L, Pearson DM, Backlund LM, Ichimura K, et al. Tandem duplication producing a novel oncogenic BRAF fusion gene defines the majority of pilocytic astrocytomas. Cancer Res. 2008;68:8673-7.
5. Pfister S, Janzarik WG, Remke M, Ernst A, Werft W, Becker N, et al. BRAF gene duplication constitutes a mechanism of MAPK pathway activation in low-grade astrocytomas. J Clin Invest. 2008;118:1739-49.
6. Jones DT, Gronych J, Lichter P, Witt O, Pfister SM. MAPK pathway activation in pilocytic astrocytoma. Cell Mol Life Sci. 2012;69:1799-811.
7. Packer RJ, Pfister S, Bouffet E, Avery R, Bandopadhayay P, Bornhorst M, et al. Pediatric low-grade gliomas: implications of the biologic era. Neuro-oncology. 2017;19:750-61.
8. Gnekow AK, Falkenstein F, von Hornstein S, Zwiener I, Berkefeld S, Bison B, et al. Long-term follow-up of the multicenter, multidisciplinary treatment study HIT-LGG-1996 for low-grade glioma in children and adolescents of the German Speaking Society of Pediatric Oncology and Hematology. Neuro-oncology. 2012;14:1265-84.
9. Jacob K, Quang-Khuong DA, Jones DT, Witt H, Lambert S, Albrecht S, et al. Genetic aberrations leading to MAPK pathway activation mediate oncogene-induced senescence in sporadic pilocytic astrocytomas. Clin Cancer Res. 2011;17:4650-60.
10. Raabe EH, Lim KS, Kim JM, Meeker A, Mao XG, Nikkhah G, et al. BRAF activation induces transformation and then senescence in human neural stem cells: a pilocytic astrocytoma model. Clinical cancer research : an official journal of the American Association for Cancer Research. 2011;17:3590-9.
11. Serrano M, Lin AW, McCurrach ME, Beach D, Lowe SW. Oncogenic ras provokes premature cell senescence associated with accumulation of p53 and p16INK4a. Cell. 1997;88:593-602.
12. Gronych J, Korshunov A, Bageritz J, Milde T, Jugold M, Hambardzumyan D, et al. An activated mutant BRAF kinase domain is sufficient to induce pilocytic astrocytoma in mice. J Clin Invest. 2011;121:1344-8.
13. Sun Y, Alberta JA, Pilarz C, Calligaris D, Chadwick EJ, Ramkissoon SH, et al. A brain-penetrant RAF dimer antagonist for the noncanonical BRAF oncoprotein of pediatric low-grade astrocytomas. Neuro-oncology. 2017;19:774-85.
14. Selt F, Hohloch J, Hielscher T, Sahm F, Capper D, Korshunov A, et al. Establishment and application of a novel patient-derived KIAA1549:BRAF-driven pediatric pilocytic astrocytoma model for preclinical drug testing. Oncotarget. 2017;8:11460-79.
15. Sengupta S, Chatterjee U, Banerjee U, Ghosh S, Chatterjee S, Ghosh AK. A study of histopathological spectrum and expression of Ki-67, TP53 in primary brain tumors of pediatric age group. Indian J Med Paediatr Oncol. 2012;33:25-31.
16. Coppe JP, Patil CK, Rodier F, Sun Y, Munoz DP, Goldstein J, et al. Senescence-associated secretory phenotypes reveal cell-nonautonomous functions of oncogenic RAS and the p53 tumor suppressor. PLoS Biol. 2008;6:2853-68.
17. Coppe JP, Desprez PY, Krtolica A, Campisi J. The senescence-associated secretory phenotype: the dark side of tumor suppression. Annu Rev Pathol. 2010;5:99-118.

18. Kuilman T, Michaloglou C, Vredeveld LC, Douma S, van Doorn R, Desmet CJ, et al. Oncogene-induced senescence relayed by an interleukin-dependent inflammatory network. Cell. 2008;133:1019-31.
19. Acosta JC, O'Loghlen A, Banito A, Guijarro MV, Augert A, Raguz S, et al. Chemokine signaling via the CXCR2 receptor reinforces senescence. Cell. 2008;133:1006-18.
20. Xue W, Zender L, Miething C, Dickins RA, Hernando E, Krizhanovsky V, et al. Senescence and tumour clearance is triggered by p53 restoration in murine liver carcinomas. Nature. 2007;445:656-60.
21. Krtolica A, Parrinello S, Lockett S, Desprez PY, Campisi J. Senescent fibroblasts promote epithelial cell growth and tumorigenesis: a link between cancer and aging. Proceedings of the National Academy of Sciences of the United States of America. 2001;98:12072-7.
22. Coppe JP, Kauser K, Campisi J, Beausejour CM. Secretion of vascular endothelial growth factor by primary human fibroblasts at senescence. The Journal of biological chemistry. 2006;281:29568-74.
23. Jones TA, Jeyapalan JN, Forshew T, Tatevossian RG, Lawson AR, Patel SN, et al. Molecular analysis of pediatric brain tumors identifies microRNAs in pilocytic astrocytomas that target the MAPK and NF-kappaB pathways. Acta Neuropathol Commun. 2015;3:86.
24. Schmitt M, Pawlita M. High-throughput detection and multiplex identification of cell contaminations. Nucleic Acids Res. 2009;37:e119.
25. Nelson DM, McBryan T, Jeyapalan JC, Sedivy JM, Adams PD. A comparison of oncogene-induced senescence and replicative senescence: implications for tumor suppression and aging. Age (Dordr). 2014;36:9637.
26. Pawlikowski JS, McBryan T, van Tuyn J, Drotar ME, Hewitt RN, Maier AB, et al. Wnt signaling potentiates nevogenesis. Proceedings of the National Academy of Sciences of the United States of America. 2013;110:16009-14.
27. Takebayashi S, Tanaka H, Hino S, Nakatsu Y, Igata T, Sakamoto A, et al. Retinoblastoma protein promotes oxidative phosphorylation through upregulation of glycolytic genes in oncogene-induced senescent cells. Aging Cell. 2015;14:689-97.
28. Ecker J, Oehme I, Mazitschek R, Korshunov A, Kool M, Hielscher T, et al. Targeting class I histone deacetylase 2 in MYC amplified group 3 medulloblastoma. Acta Neuropathol Commun. 2015;3:22.
29. Smyth GK. Linear models and empirical bayes methods for assessing differential expression in microarray experiments. Stat Appl Genet Mol Biol. 2004;3:Article3.
30. Smyth GK. Limma: linear models for microarray data. In: R. Gentleman VC, S. Dudoit, R. Irizarry, W. Humber, editor. Bioinformatics and Computational Biology Solutions using R and Bioconductor. New York: Springer; 2005. p. 397-420.
31. Breitling R, Armengaud P, Amtmann A, Herzyk P. Rank products: a simple, yet powerful, new method to detect differentially regulated genes in replicated microarray experiments. FEBS Lett. 2004;573:83-92.
32. Eisinga R, Breitling R, Heskes T. The exact probability distribution of the rank product statistics for replicated experiments. FEBS Lett. 2013;587:677-82.
33. Wu D, Smyth GK. Camera: a competitive gene set test accounting for inter-gene correlation. Nucleic Acids Res. 2012;40:e133.
34. Li Q, Birkbak NJ, Gyorffy B, Szallasi Z, Eklund AC. Jetset: selecting the optimal microarray probe set to represent a gene. BMC Bioinformatics. 2011;12:474.
35. Gravendeel LA, Kouwenhoven MC, Gevaert O, de Rooi JJ, Stubbs AP, Duijm JE, et al. Intrinsic gene expression profiles of gliomas are a better predictor of survival than histology. Cancer Res. 2009;69:9065-72.
36. Sharma MK, Mansur DB, Reifenberger G, Perry A, Leonard JR, Aldape KD, et al. Distinct genetic signatures among pilocytic astrocytomas relate to their brain region origin. Cancer Res. 2007;67:890-900.
37. Lambert SR, Witt H, Hovestadt V, Zucknick M, Kool M, Pearson DM, et al. Differential expression and methylation of brain developmental genes define location-specific subsets of pilocytic astrocytoma. Acta neuropathologica. 2013;126:291-301.

38. Orjalo AV, Bhaumik D, Gengler BK, Scott GK, Campisi J. Cell surface-bound IL-1alpha is an upstream regulator of the senescence-associated IL-6/IL-8 cytokine network. Proceedings of the National Academy of Sciences of the United States of America. 2009;106:17031-6.
39. Kumar S, Millis AJ, Baglioni C. Expression of interleukin 1-inducible genes and production of interleukin 1 by aging human fibroblasts. Proceedings of the National Academy of Sciences of the United States of America. 1992;89:4683-7.
40. Uekawa N, Nishikimi A, Isobe K, Iwakura Y, Maruyama M. Involvement of IL-1 family proteins in p38 linked cellular senescence of mouse embryonic fibroblasts. FEBS Lett. 2004;575:30-4.
41. Dinarello CA. The many worlds of reducing interleukin-1. Arthritis Rheum. 2005;52:1960-7.
42. Yamin TT, Miller DK. The interleukin-1 receptor-associated kinase is degraded by proteasomes following its phosphorylation. The Journal of biological chemistry. 1997;272:21540-7.
43. Chien Y, Scuoppo C, Wang X, Fang X, Balgley B, Bolden JE, et al. Control of the senescence-associated secretory phenotype by NF-kappaB promotes senescence and enhances chemosensitivity. Genes Dev. 2011;25:2125-36.
44. Adler AS, Sinha S, Kawahara TL, Zhang JY, Segal E, Chang HY. Motif module map reveals enforcement of aging by continual NF-kappaB activity. Genes Dev. 2007;21:3244-57.
45. Zohlnhofer D, Graeve L, Rose-John S, Schooltink H, Dittrich E, Heinrich PC. The hepatic interleukin-6 receptor. Down-regulation of the interleukin-6 binding subunit (gp80) by its ligand. FEBS Lett. 1992;306:219-22.
46. Zhong Z, Wen Z, Darnell JE, Jr. Stat3: a STAT family member activated by tyrosine phosphorylation in response to epidermal growth factor and interleukin-6. Science. 1994;264:95-8.
47. Starr R, Willson TA, Viney EM, Murray LJ, Rayner JR, Jenkins BJ, et al. A family of cytokine-inducible inhibitors of signalling. Nature. 1997;387:917-21.
48. Hiscott J, Marois J, Garoufalis J, D'Addario M, Roulston A, Kwan I, et al. Characterization of a functional NF-kappa B site in the human interleukin 1 beta promoter: evidence for a positive autoregulatory loop. Mol Cell Biol. 1993;13:6231-40.
49. Laberge RM, Zhou L, Sarantos MR, Rodier F, Freund A, de Keizer PL, et al. Glucocorticoids suppress selected components of the senescence-associated secretory phenotype. Aging Cell. 2012;11:569-78.
50. Ge H, Ke J, Xu N, Li H, Gong J, Li X, et al. Dexamethasone alleviates pemetrexed-induced senescence in Non-Small-Cell Lung Cancer. Food Chem Toxicol. 2018.
51. Baar MP, Brandt RMC, Putavet DA, Klein JDD, Derks KWJ, Bourgeois BRM, et al. Targeted Apoptosis of Senescent Cells Restores Tissue Homeostasis in Response to Chemotoxicity and Aging. Cell. 2017;169:132-47 e16.
52. Montero J, Letai A. Why do BCL-2 inhibitors work and where should we use them in the clinic? Cell Death Differ. 2018;25:56-64.
53. Bavik C, Coleman I, Dean JP, Knudsen B, Plymate S, Nelson PS. The gene expression program of prostate fibroblast senescence modulates neoplastic epithelial cell proliferation through paracrine mechanisms. Cancer Res. 2006;66:794-802.
54. Jing H, Kase J, Dorr JR, Milanovic M, Lenze D, Grau M, et al. Opposing roles of NF-kappaB in anti-cancer treatment outcome unveiled by cross-species investigations. Genes Dev. 2011;25:2137-46.

Figure 1

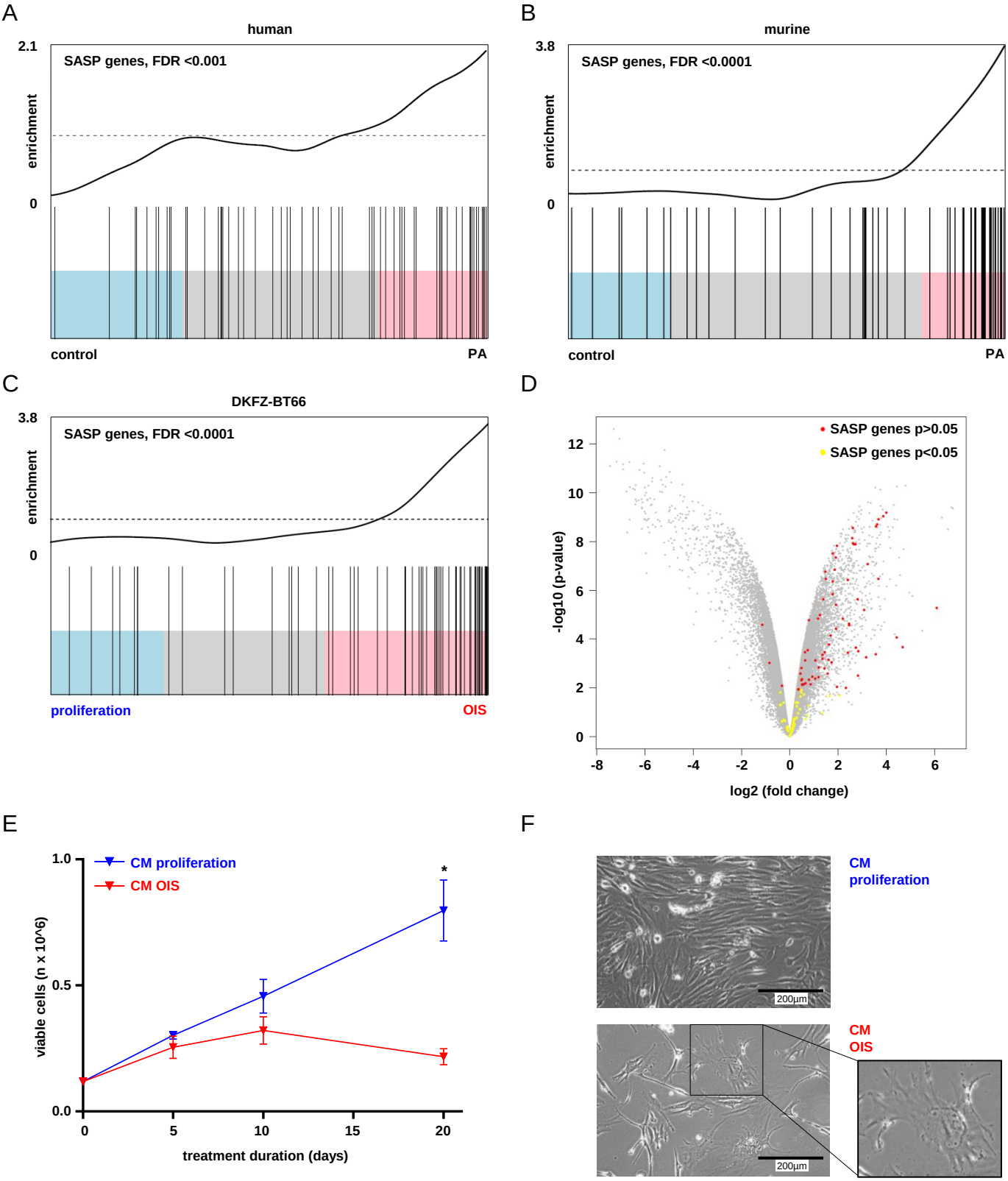
A
human
SASP genes, FDR <0.001
2.1
enrichment
0
control
PA
B
murine
SASP genes, FDR <0.0001
3.8
enrichment
0
control
PA
C
DKFZ-BT66
SASP genes, FDR <0.0001
3.8
enrichment
0
proliferation
OIS
D
SASP genes p>0.05
SASP genes p<0.05
-log10 (p-value)
log2 (fold change)
E
CM proliferation
CM OIS
viable cells (n x 10^6)
treatment duration (days)
F
CM proliferation
CM OIS
200µm
200µm

Figure 2

A

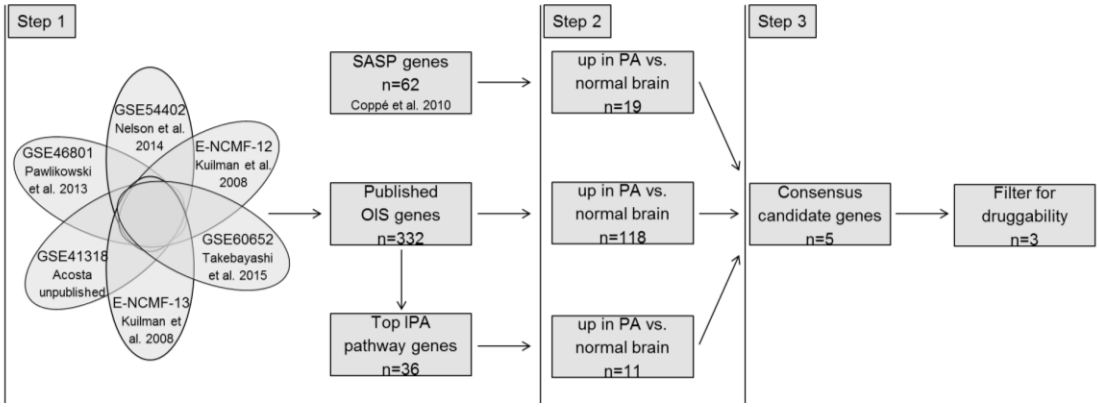

B

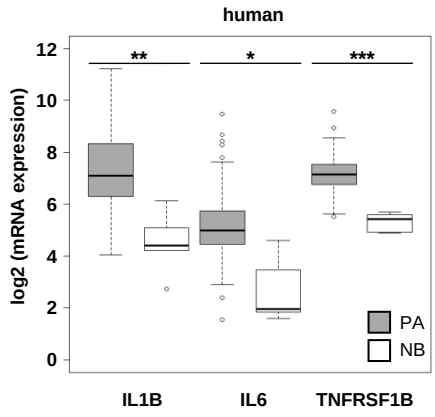

C

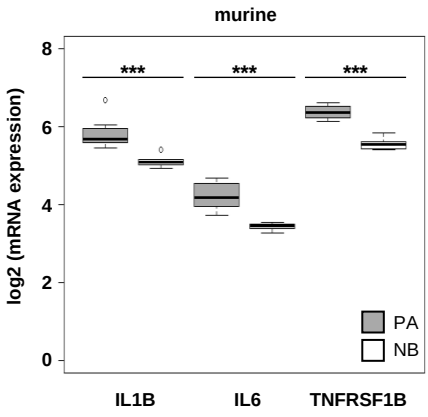

D

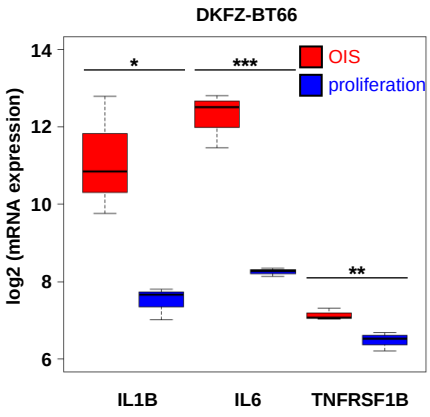

E

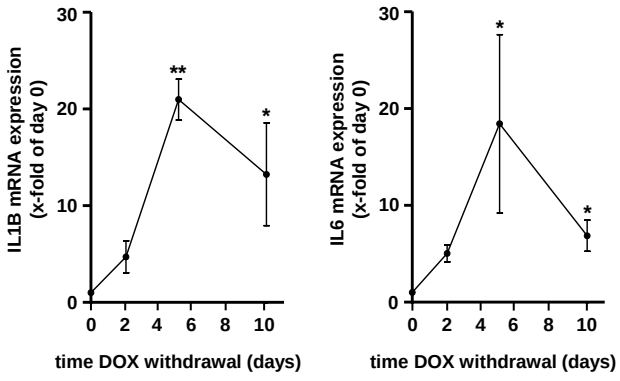

F

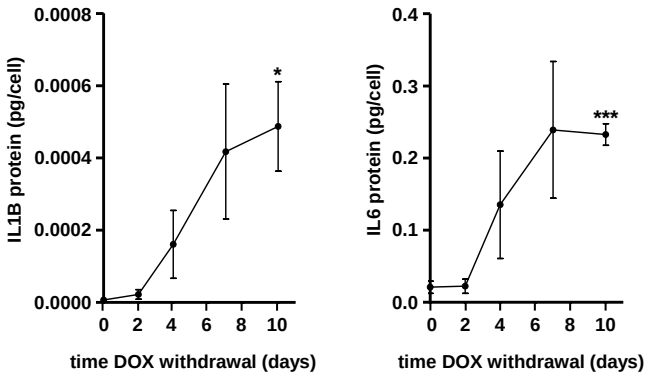

Figure 3

A

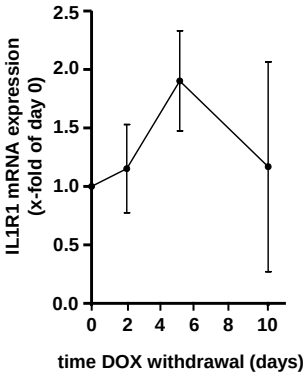

B

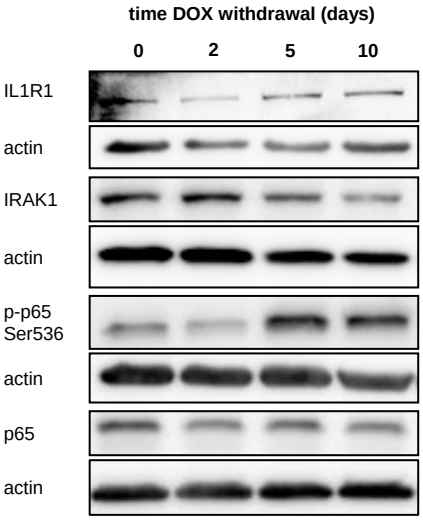

C

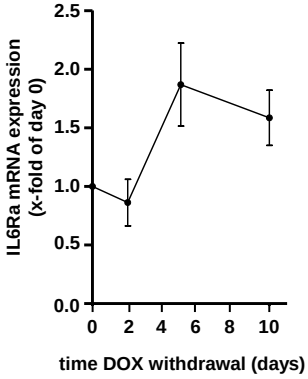

D

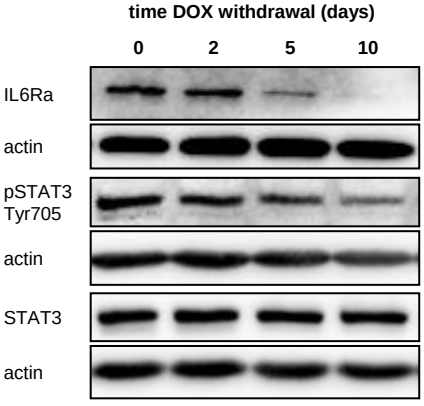

E

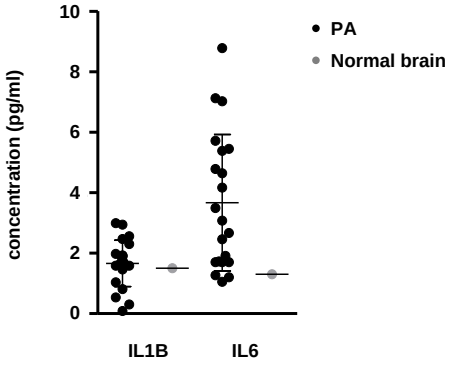

Figure 4

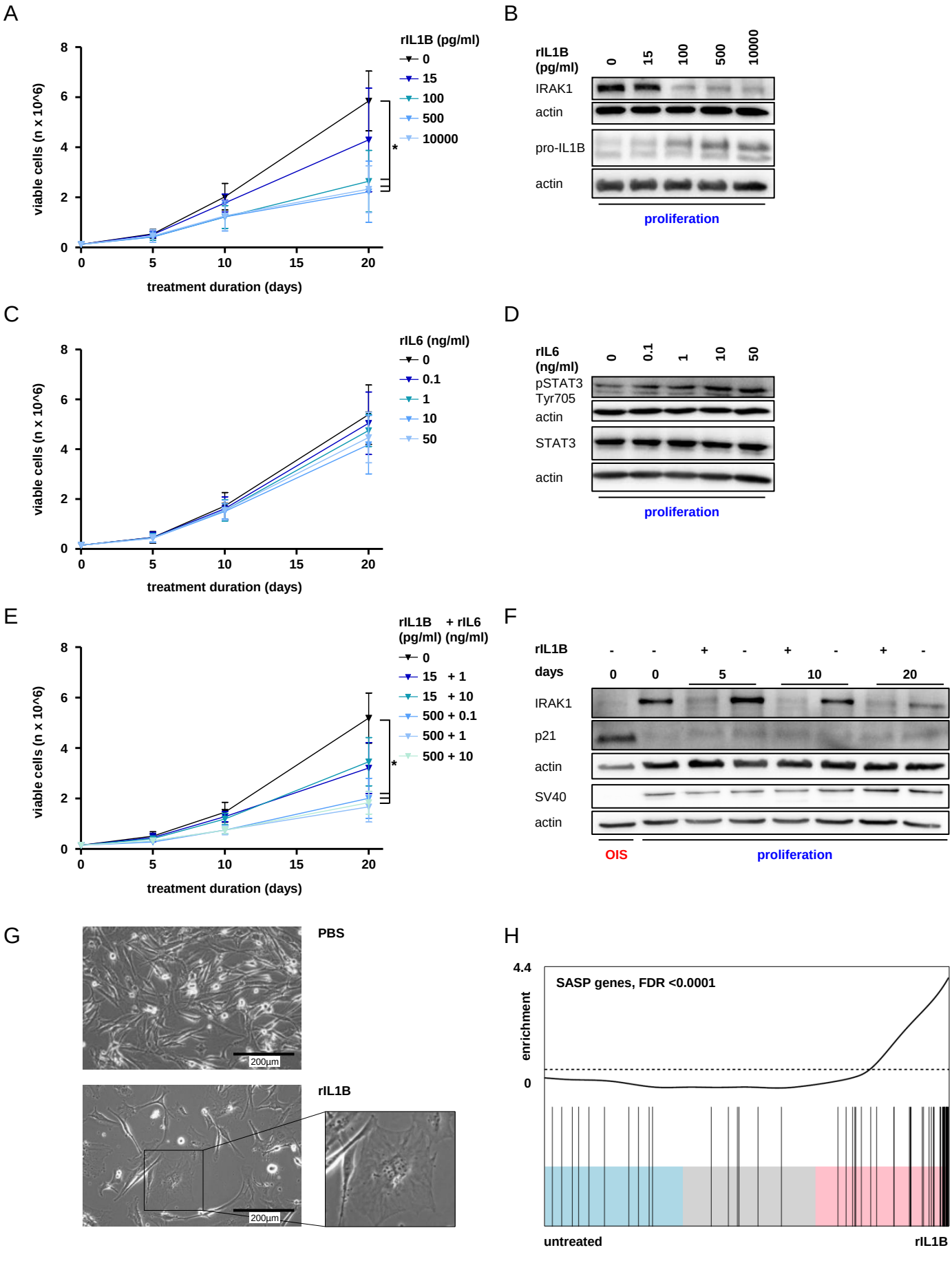
A
viable cells (n x 10^6)
treatment duration (days)
rIL1B (pg/ml)
0
15
100
500
10000
*
B
rIL1B (pg/ml)
0
15
100
500
10000
IRAK1
actin
pro-IL1B
actin
proliferation
C
viable cells (n x 10^6)
treatment duration (days)
rIL6 (ng/ml)
0
0.1
1
10
50
D
rIL6 (ng/ml)
0
0.1
1
10
50
pSTAT3 Tyr705
actin
STAT3
actin
proliferation
E
viable cells (n x 10^6)
treatment duration (days)
rIL1B (pg/ml)
+ rIL6 (ng/ml)
0
15 + 1
15 + 10
500 + 0.1
500 + 1
500 + 10
*
F
rIL1B
days
IRAK1
p21
actin
SV40
actin
OIS
proliferation
G
PBS
200µm
rIL1B
200µm
H
4.4
enrichment
0
SASP genes, FDR <0.0001
untreated
rIL1B

Figure 5

A

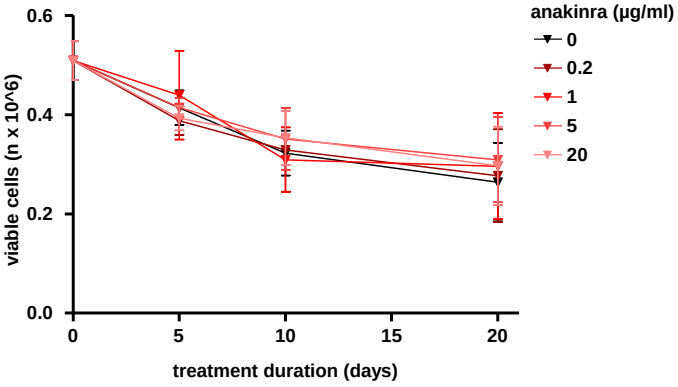

B

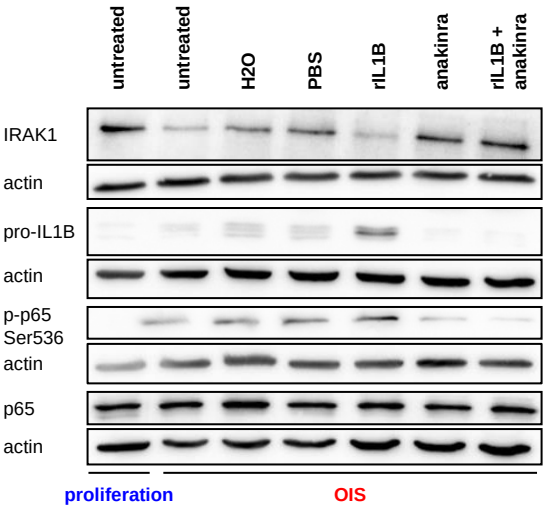

C

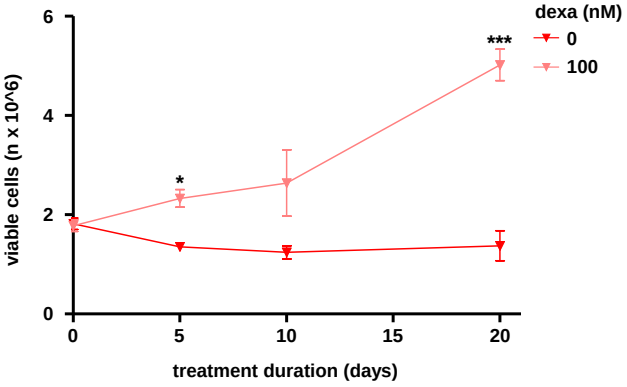

D

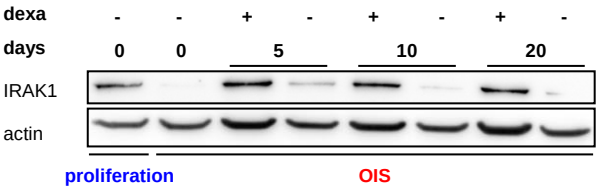

E

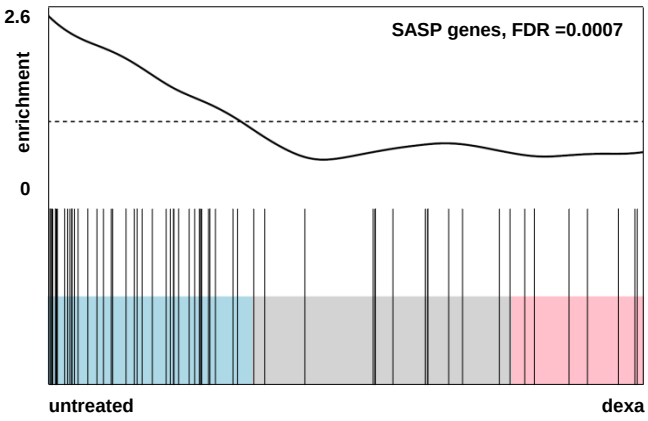

F

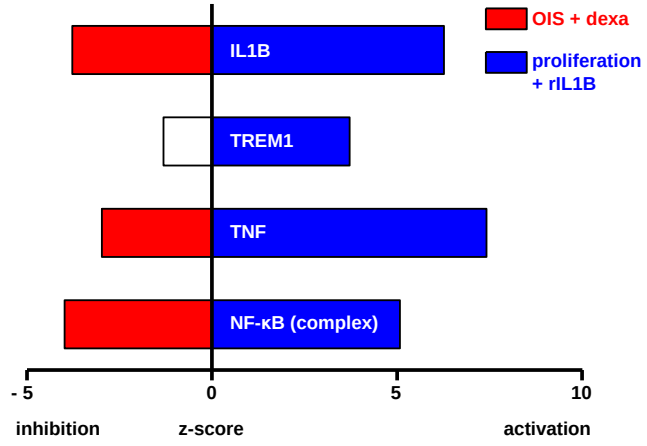

Figure 6

A

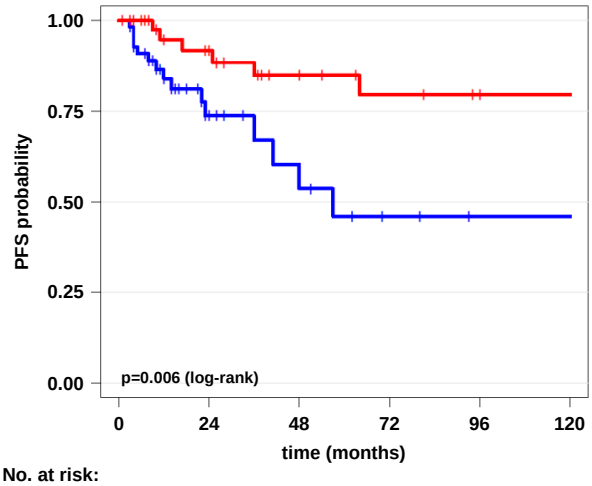

No. at risk:						
IL1B low:	56	17	9	4	2	2
IL1B high:	54	29	21	15	12	11

B

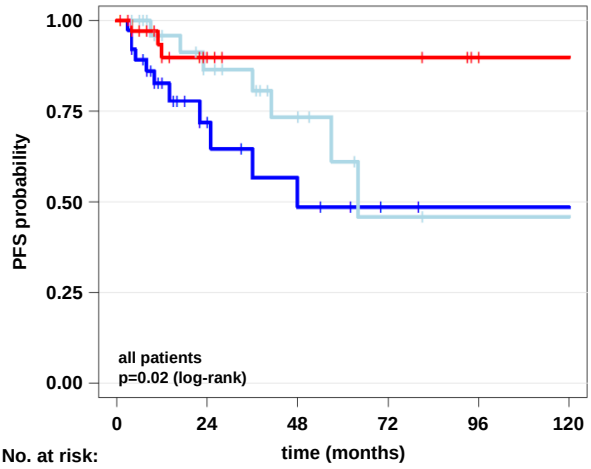

No. at risk:						
SASP low:	38	11	7	3	2	2
SASP intermediate:	35	17	10	3	2	2
SASP high:	37	18	13	13	10	9

C

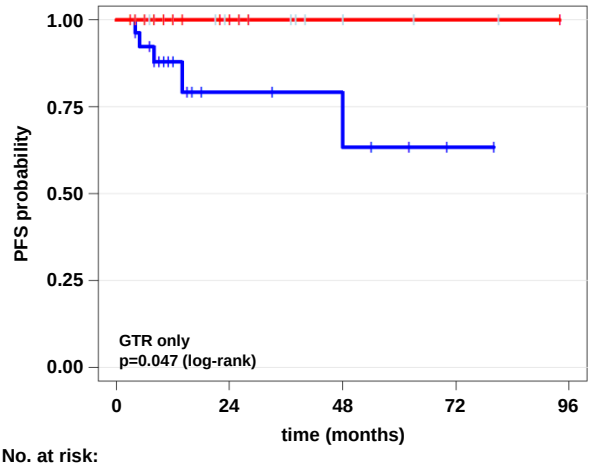

No. at risk:					
SASP low:	27	6	5	1	0
SASP intermediate:	19	8	3	1	0
SASP high:	15	4	1	1	0

D

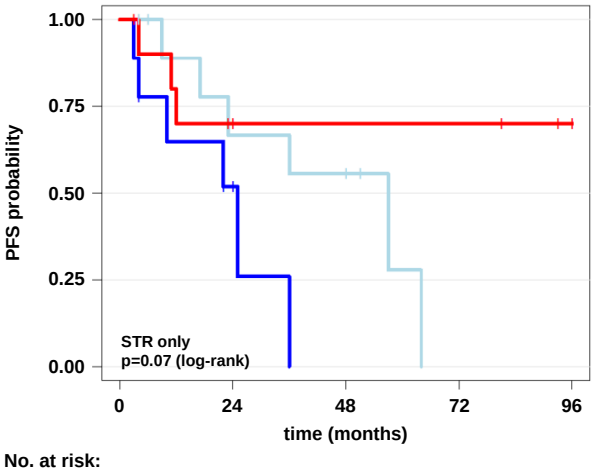

No. at risk:					
SASP low:	9	3	0	0	0
SASP intermediate:	12	6	5	0	0
SASP high:	11	5	3	3	1

Figure 7

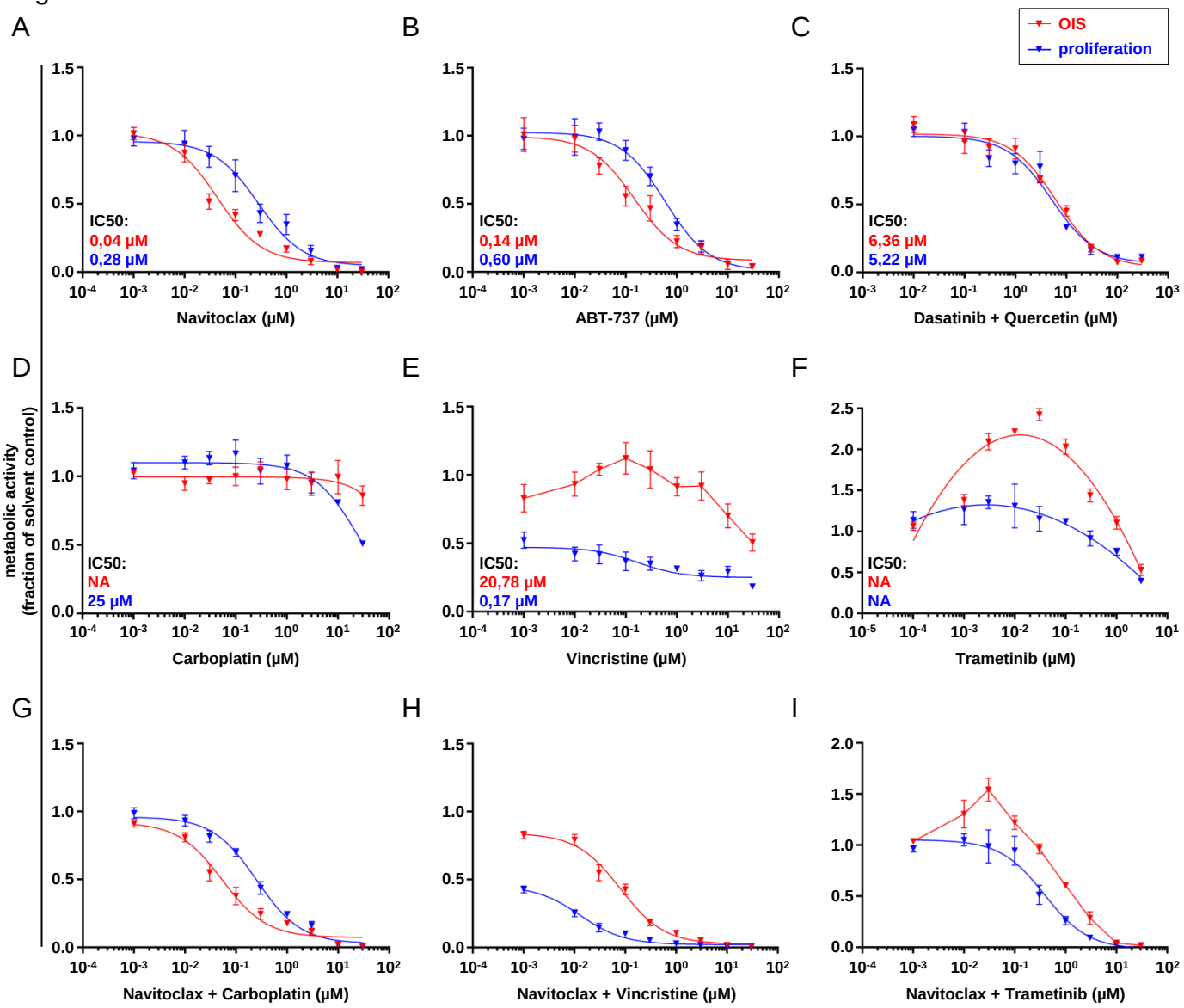
A
B
C
OIS
proliferation
IC50:
0,04 µM
0,28 µM
Navitoclax (µM)
IC50:
0,14 µM
0,60 µM
ABT-737 (µM)
IC50:
6,36 µM
5,22 µM
Dasatinib + Quercetin (µM)
D
E
F
metabolic activity
(fraction of solvent control)
IC50:
NA
25 µM
Carboplatin (µM)
IC50:
20,78 µM
0,17 µM
Vincristine (µM)
IC50:
NA
NA
Trametinib (µM)
G
H
I
Navitoclax + Carboplatin (µM)
Navitoclax + Vincristine (µM)
Navitoclax + Trametinib (µM)